Journal of Photochemistry, 21 (1983) 281 - 289

ELECTRONIC QUENCHING OF CH(A $^2\Delta$–X $^2\Pi$) AND OH (A $^2\Sigma^+$–X $^2\Pi$) BY N_2 AND O_2

F. L. TABARÉS and A. GONZÁLEZ UREÑA

Departamento de Química Fisica, Facultad de Químicas, Universidad Complutense de Madrid, Madrid 3 (Spain)

(Received July 13, 1982; in revised form September 25, 1982)

Summary

The electronic quenching of excited CH(A $^2\Delta$) and OH(A $^2\Sigma^+$) by N_2 and O_2 was measured using reactive $O(^3P)$–C_6H_6 mixtures in a fast flow reactor to produce the excited radicals. The rate constant data for both O_2 and N_2 quenching of the two OH($^2\Sigma^+$) and CH(A $^2\Delta$) excited species were found to be $k_q(CH^* + O_2) = 2.2 \times 10^{14}$ mol^{-1} cm^3 s^{-1}, $k_q(CH^* + N_2) = 1.7 \times 10^{13}$ mol^{-1} cm^3 s^{-1}, $k_q(OH^* + O_2) = 2.1 \times 10^{14}$ mol^{-1} cm^3 s^{-1} and $k_q(OH^* + N_2) = 1.0 \times 10^{13}$ mol^{-1} cm^3 s^{-1}.

1. Introduction

A study of the CH* and OH* chemiluminescent radiations produced in $O(^3P)$–C_6H_6 reactive mixtures performed using our discharge fast flow apparatus was reported in a previous paper [1]. Both emissions were identified as the CH(A $^2\Delta$–X $^2\Pi$) and OH(A $^2\Sigma^+$–X $^2\Pi$) electronic transitions and were monitored as a function of the reactant concentrations and the experimental conditions. However, no consideration was given to their physical and chemical quenching by different gases and this is the main purpose of this paper.

To date only a few determinations of the quenching of excited CH* and OH* radicals by different species have been reported [2 - 4]. In this paper the values of the rate constants for physical quenching by N_2 are completed and new data on the (physical and chemical) electronic quenching by O_2 of these two excited radicals which are involved in many interesting atmospheric and combustion reactions are given.

The experimental technique and conditions are described briefly in Section 2. The results and data analysis are presented in Section 3 and a discussion with some concluding remarks is given in Section 4.

0047-2670/83/0000-0000/$03.00

2. Experimental details

The experimental arrangement has been described in detail elsewhere [1, 5, 6] and only a brief description will be presented here. The experimental conditions are given in Table 1. Our apparatus consists of a Pyrex reactor pumped with a strong mechanical pump to produce a fast flow velocity of several thousand centimetres per second. The flow system is of a conventional design with the gas flows controlled by needle valves and measured using a calibrated floating-ball flowmeter of the type employed with organic (aromatic) compounds. The typical benzene flow range in the present experiment was 6.8 - 15.8 μmol s^{-1}. The main gas flow (0.7 - 1.3 mmol Ar s^{-1} and 70 - 140 μmol N_2O s^{-1}) was passed through a modulated discharge cavity powered by a microwave unit where the $O(^3P)$ atoms were produced before entering the flow tube. The Pyrex reactor wall was coated with boric acid to minimize the O atom recombination with the wall. Since the O atoms in the present experiment were produced by modulated discharge any emission from the reaction products would obviously be modulated at the same frequency as the discharge. As the reactants are introduced into the reactor inlet the reaction between the O atoms and the organic compound takes place and any chemiluminescent products formed are detected by measuring the emission intensity.

After identification of the emission band the OH* and CH* intensities were recorded as a function of the concentrations of the reactants and the O_2 or N_2 (quencher). The reactants were mixed before the observation zone and the quencher inlet was located in front of this point, *i.e.* in front of the monochromator side view, so that in a normal run the number of oxygen atoms, the benzene concentration and the temperature were fixed and only the quencher concentration, *i.e.* either $[N_2]$ or $[O_2]$, was changed.

TABLE 1

Experimental conditions

Gas flow (μmol s^{-1})	
Ar	1300
N_2O	140
C_6H_6	6.8 - 15.8
Total pressure (Torr)	2.0
Temperature (K)	333
Discharge frequency (Hz)	42.5
Discharge power (W)	100
Reaction time (ms)	7.0
Photomultiplier voltage (V)	1800
Typical signal [a] (μV)	2×10^{-3} - 10^{-2}
Typical noise [a] (μV)	10^{-4}
Monochromator resolution (nm)	8
Quencher concentration ($\times 10^8$ mol cm^{-3})	0.16 - 6.0

[a] The range of values depends on the benzene concentration range.

3. Results

3.1. Data

Figure 1 shows the CH* and OH* emission intensities as functions of the N_2 and O_2 concentrations at fixed initial oxygen and benzene concentrations. The behaviour of the emitting species was examined further by performing a series of experiments (with [O] fixed) in which both the C_6H_6 and the O_2 concentrations were changed and the OH* and CH* emission intensities were recorded. The results are shown in Fig. 2. It should be noted that the data in Fig. 2 are plotted using the empirical functions reported in ref. 1, *i.e.* $\ln(I/[B]^n)$ is plotted against [B] where I is the CH* or OH* emission intensity, [B] is the benzene concentration and $n = 1$ for CH* emission and $n = 2$ for OH* emission. As we shall discuss later it is important to note that the slopes of the $\ln(I/[B]^n)$ plots do not vary much with increasing O_2 concentration.

Comparison of the plots for N_2 and O_2 quenching indicates that (a) a similar slope is obtained for the N_2 quenching of both CH* and OH*, (b) O_2 quenching yields a steeper slope than N_2 quenching for both CH* and OH* and (c) the slope for O_2 quenching of CH* is steeper than that for quenching of OH*.

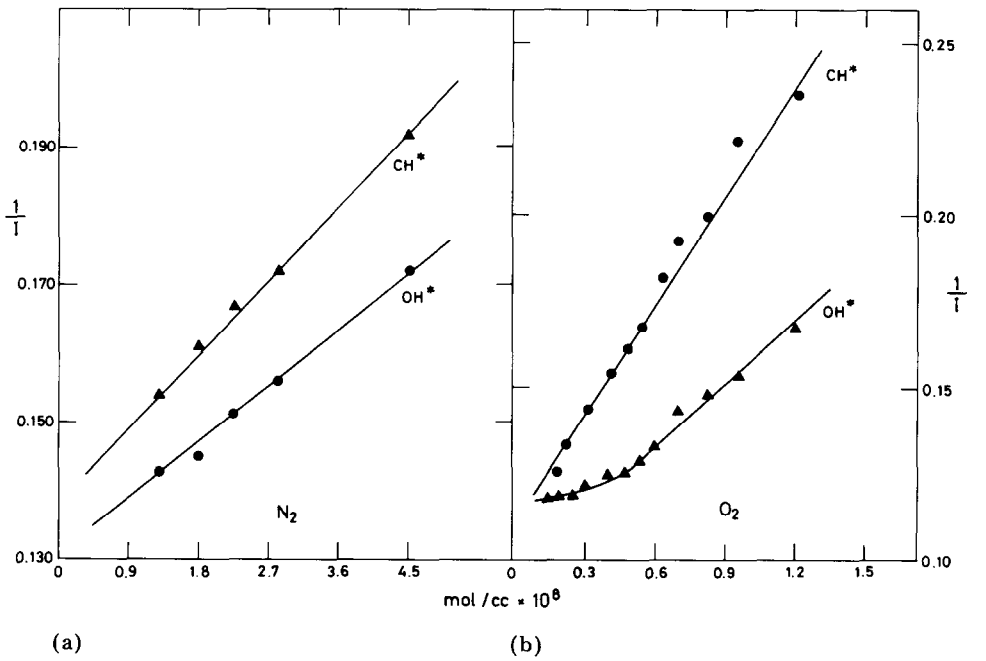

Fig. 1. Stern–Volmer plots of CH* and OH* emission intensities as a function of (a) $[N_2]$ and (b) $[O_2]$: ——, curves fitted to the data points.

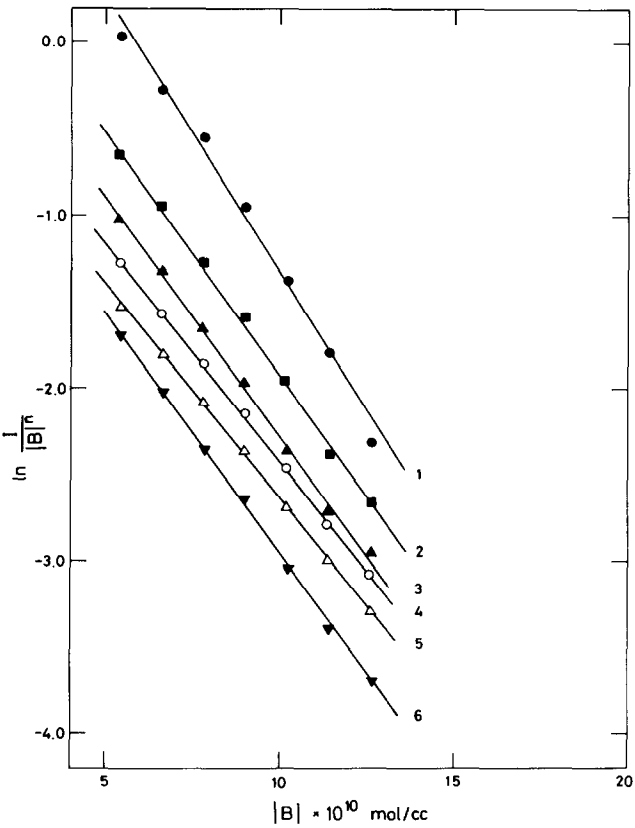

Fig. 2. CH* (curves 1 - 3) and OH* (curves 4 - 6) emission intensities at T = 330 K as functions of [B] and [O_2]: curves 1 and 6, [O_2] = 0 mol cm^{-3}; curves 2 and 4, [O_2] = 4.2×10^{-8} mol cm^{-3}; curves 3 and 5, [O_2] = 6×10^{-8} mol cm^{-3}. The ordinate shows $\ln(I/[B]^n)$ where n = 1 for CH* emission and n = 2 for OH* emission [1].

3.2. Quenching mechanisms and data analysis

The general scheme shown in Table 2 can be established for the quenching mechanism under our experimental conditions. In Table 2 X* stands for either OH* or CH* and the summation over i is extended to all the quenchers present in the experiments, *e.g.* argon and C_6H_6, in addition to the specific quencher Q ≡ N_2, O_2. The steady state approximation for [X*] can be expressed as

$$[X^*]_{ss} = \frac{f}{k_q[Q] + k_F + \Sigma_i k_q^i[M_i]}$$

which when introduced in the expression $I_{X^*} = k_F[X^*]$ for the emission intensity gives

$$\frac{I_{X^*}^0}{I_{X^*}} = 1 + \frac{k_q[Q]}{k_F + \Sigma_i k_q^i[M_i]} \qquad (1)$$

TABLE 2

Reaction	*Process*	*Rate*
Reactants → X*	Formation	*f*(reactants)
X* + Q → products	Specific quenching	$k_q[Q][X^*]$
X* + M_i → X + M_i → products	General (physical and/or chemical) quenching	$\Sigma_i k_q^i[M_i][X^*]$
X* → X + $h\nu$	Fluorescence	$k_F[X^*]$

where $I_{X^*}{}^0$ is the emission intensity in the absence of Q, *i.e.*

$$I_{X^*}{}^0 = \frac{k_F f}{k_F + \Sigma_i k_q{}^i[M_i]}$$

Equation (1) can be arranged in the Stern–Volmer form, *i.e.*

$$\frac{1}{I_{X^*}} = \frac{1}{I_{X^*}{}^0}\left(1 + \frac{k_q[Q]}{k_F + \Sigma_i k_q{}^i[M_i]}\right) \tag{2}$$

which can be used to plot the variation of the emission intensity with [Q] when the concentrations of the other quenchers are kept constant. The electronic quenching of CH* and OH* by argon can be neglected under our experimental conditions because k_F is much greater than $k_q{}^{Ar}[Ar]$ in each case. Typically $[Ar] \approx 1 \times 10^{-7}$ mol cm^{-3} and the measured values of $k_q{}^{Ar}$ and k_F [2, 3] show that $k_q{}^{Ar}[Ar] \approx 5 \times 10^4 \ll k_F$. Thus the summation in eqn. (2) reduces to $k_q{}^B[B]$. When eqn. (2) is used to analyse the quenching emission data we find that the slope-to-intercept ratio is given by $k_q/(k_F + k_q{}^B[B])$.

The data analysis shown in Fig. 1 which was obtained by plotting the emission intensity according to eqn. (1) allows us to determine the quenching constant once k_F and $k_q{}^B$ are known.

At this point it should be noted that within the benzene concentration range studied here $k_q{}^B[B]$ is much less than k_F. Evidence for this can be obtained from Fig. 2 where it can be seen that the slopes of the plots of $\ln(I_{X^*}/[B]^n)$ *versus* [B] for various values of $[O_2]$ are almost the same. Therefore we can assume that the "experimental" slope-to-intercept ratios obtained from Fig. 1 are given by $S \approx k_q/k_F$ and k_q can be obtained once the literature value of k_F is substituted. The k_q values determined in this way are listed in Table 3 together with some earlier determinations.

The same procedure can be adopted for the quenching of the CH* emission intensity by O_2 but now the rate constant is the sum of both the physical and the chemical quenching contributions, *i.e.* $k_q{}^{O_2}(\text{total}) = k_r{}^{O_2} + k_q{}^{O_2}$ because in our experiments both processes occur simultaneously without any possibility of separation. The value thus obtained is 2.2×10^{14} cm^3 mol^{-1} s^{-1} which can be considered as an upper limit for $k_r{}^{O_2}$ because it is expected that $k_q{}^{O_2}$ will be of a similar order of magnitude to $k_q{}^{N_2}$.

TABLE 3

Rate constants for the physical and chemical quenching of CH(A $^2\Delta$) and OH(A $^2\Sigma^+$) at 330 K

Species	*Quencher*	k (cm^3 mol^{-1} s^{-1})	
		This work	*Previous work*
OH*	N_2	$(1.0 \pm 0.1) \times 10^{13}$	3×10^{12} - 3×10^{13} [2]
	Ar	—	1.2×10^{11} - 8.4×10^{12} [2]
	O_2	$(2.1 \pm 0.2) \times 10^{14}$	1.42×10^{14} [3]
CH*	N_2	$(1.7 \pm 0.2) \times 10^{13}$	2.0×10^{13} [4]
	O_2	$(2.2 \pm 0.2) \times 10^{14}$	

Since one of the mechanisms of the O_2 quenching of CH* is in fact a new source of OH*, *i.e.* CH* + $O_2 \rightarrow$ OH* + CO, the OH* mechanism must be changed by including this new reaction. Therefore the final scheme is as given in Table 4. The steady state approximation for OH* gives

$$[OH^*]_{ss} = \frac{f + k_r'[CH^*][O_2]}{k_q[O_2] + \Sigma_i k_q^i[M_i] + k_F}$$

and

$$I_{OH^*} = k_F[OH^*]_{ss}$$

TABLE 4

Process	*Rate*
Reactants $\rightarrow$ OH*	f(reactants)
CH* + $O_2 \rightarrow$ CO + OH*	$k_r'[CH^*][O_2]$
OH* + $O_2 \rightarrow$ products	$k_q[O_2][OH^*]$
OH* + $M_i \rightarrow$ products	$\Sigma_i k_q^i[M_i][OH^*]$
$\rightarrow$ OH + M_i	
OH* $\rightarrow$ OH + $h\nu$	$k_F[OH^*]$

In the absence of O_2 in the reaction mixture, the OH* intensity $I_{OH^*}^0$ is given by

$$I_{OH^*}^0 = \frac{k_F f}{k_F + \Sigma_i k_q^i[M_i]}$$

Assuming again that $\Sigma_i k_q^i[M_i]$ is much less than k_F, we obtain

$$I_{OH^*} = \frac{k_F I_{OH^*}^0 + k_F k_r'[CH^*][O_2]}{k_q[O_2] + k_F}$$

Since $I_{CH^*} = k_F'[CH^*]$, where k_F' is the rate constant of the CH* fluorescence, we obtain

$$I_{OH^*} = \frac{I_{OH^*}{}^0 + k_r' I_{CH^*}[O_2]/k_F'}{1 + (k_q/k_F)[O_2]}$$

which can be rearranged to give

$$\frac{I_{OH^*}{}^0 - I_{OH^*}}{[O_2] I_{OH^*}} = -\frac{k_r'}{k_F'} \frac{I_{CH^*}}{I_{OH^*}} + \frac{k_q}{k_F} \tag{3}$$

i.e. a different equation from that given previously which explains the anomalous behaviour (the curvature at low O_2 concentration) observed for OH* in Fig. 1(b).

A plot of the left-hand side of eqn. (3) *versus* I_{CH^*}/I_{OH^*} should give a straight line with intercept k_q/k_F. Appropriate normalization of both emission intensities should also give an approximate value for k_q/k_F. Figure 3 shows the relation between $(I_{OH^*}{}^0 - I_{OH^*})/[O_2]I_{OH^*}$ and I_{CH^*}/I_{OH^*}. A linear relation is obtained as expected. Since we are more interested in determining k_q/k_F from the intercept the as-measured experimental I_{CH^*}/I_{OH^*} ratio, *i.e.* without any scaling or normalization to account for the different wavelengths and apparatus responses to the emissions, is plotted on the abscissa. A k_q value of 2.15×10^{14} cm^3 mol^{-1} s^{-1} was obtained ($k_F = 1.45 \times 10^6$ s^{-1} [2]). In addition, by considering the experimentally observed I_{CH^*}/I_{OH^*} ratio of 1.5 in the absence of a quencher we obtain from the slope of Fig. 3 a k_r' value of 2.18×10^{14} cm^3 mol^{-1} s^{-1} which is consistent with our previous determination. Our present values are summarized and compared with values determined previously in Table 3.

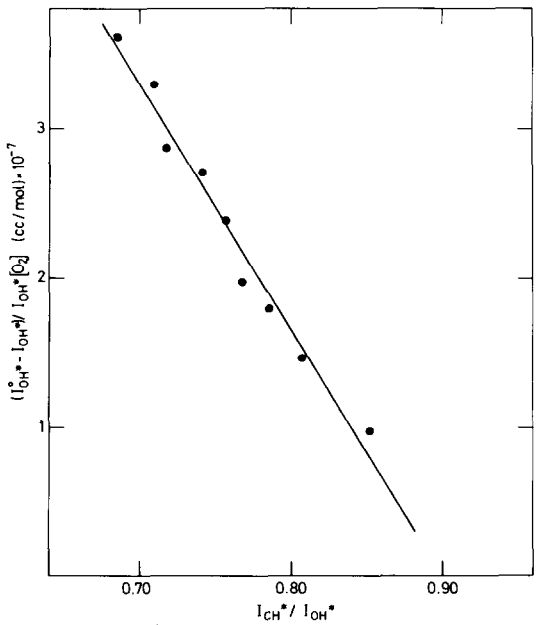

Fig. 3. $(I_{OH^*}{}^0 - I_{OH^*})/[O_2]I_{OH^*}$ *vs.* I_{CH^*}/I_{OH^*} (eqn. (3)): •, experimental data; ——, representation obtained using the linear relations shown in Fig. 2 for the emission intensities of CH* and OH*.

4. Discussion

Some discussion of the quenching rate constants reported in Table 3 is necessary. First it should be noted that the N_2 quenching constants determined in this work are similar to those measured previously which suggests that, at least for the experiments reported here, the method is satisfactory even for excited species (OH* and CH*) produced via a fast flow chemical reaction.

However, the O_2 quenching experiment needs more detailed consideration because of (a) the presence of the $CH^* + O_2 \rightarrow OH^* + CO$ reaction and (b) the question of whether OH*, CH* or one of their precursors is being quenched. The observation that the total O_2 quenching rate constant for OH* is larger than the N_2 quenching rate constant indicates that fast chemical reactions involving O_2 as a reactant are responsible for the total (observed) quenching. Krishnamachari and Broida [7] observed a large increase in OH* emission (accompanied by a decrease in C_2^* and CH* emissions) in an oxyacetylene flame when O_2 was added to the reactive mixture, thus confirming the mechanism $CH^* + O_2 \rightarrow OH^* + CO$ suggested earlier for the production of the excited hydroxyl radical. In the present experiment the observation of the OH* emission when either (a) N_2O (instead of O_2) is discharged or (b) the $N + NO \rightarrow N_2 + O$ reaction is used as a source of oxygen atoms suggests that another mechanism in addition to the $CH^* + O_2 \rightarrow CO + OH^*$ reaction is responsible for the formation of $OH(^2\Sigma^+)$ as suggested in our previous study. Brennen and Carrington [4] have studied the quenching of $CH(A\ ^2\Delta)$ by O_2 in the $O + C_2H_2$ reaction. They showed that the quenching behaviour could be quite well represented by Stern–Volmer equations but that the effective reaction cross section was greater than 1000 $Å^2$ from which they concluded that the quenching occurs by the reaction of the added O_2 with an unknown CH* precursor rather than by direct reaction with CH* itself. In the results reported here the slopes of the $\ln(I/[B]^n)$ plots for CH* and OH* change little with increasing O_2 concentration (Fig. 2) and hence we can conclude that O_2 does not play an important role in the formation of either CH* or OH*. The major influence of O_2 is as a chemical or physical quencher once the excited species are formed. Our "experimental" value of about 13 $Å^2$ for the reactive cross section σ of the O_2 quenching of CH* obtained from the rate constants in Table 3 provides further evidence for the proposal that this quenching takes place via a direct reaction of the excited $CH(A\ ^2\Delta)$ species.

Acknowledgment

This work received financial support from the Comision Asesora of Spain.

References

1 F. L. Tabarés, J. Sáez Rábanos and A. González Ureña, *J. Chem. Soc., Faraday Trans. I, 78* (1982) 3679.
2 P. Hogan and D. D. Davis, *J. Chem. Phys., 62* (1975) 4574.
3 H. P. Hooymayers and C. Th. J. Alkemake, *J. Quant. Spectrosc. Radiat. Transfer, 7* (1967) 495.
4 W. Brennen and T. Carrington, *J. Chem. Phys., 46* (1967) 7.
5 A. González Ureña, F. Tabarés and V. Sáez Rábanos, *Physico-Chemical Hydrodynamics 3, Madrid, March 1980, Europhysics Conf. Abstr. 3F*, 1980, p. 144 (European Physical Society).
6 V. Sáez Rábanos, F. Tabarés and A. González Ureña, *J. Photochem., 18* (1982) 301.
7 S. L. N. G. Krishnamachari and H. P. Broida, *J. Chem. Phys., 34* (1961) 1709.